Extreme Maximum Land Surface Temperatures

J. R. GARRATT

CSIRO, Division of Atmospheric Research, Melbourne, Australia

(Manuscript received 17 September 1991, in final form 18 December 1991)

ABSTRACT

There are numerous reports in the literature of observations of land surface temperatures. Some of these, almost all made in situ, reveal maximum values in the 50°–70°C range, with a few, made in desert regions, near 80°C. Consideration of a simplified form of the surface energy balance equation, utilizing likely upper values of absorbed shortwave flux ($\approx$1000 W m^{-2}) and screen air temperature ($\approx$55°C), suggest that surface temperatures in the vicinity of 90°–100°C may occur for dry, darkish soils of low thermal conductivity ($\approx$0.1–0.2 W m^{-1} K^{-1}). Numerical simulations confirm this and suggest that temperature gradients in the first few centimeters of soil may reach 0.5°–1°C mm^{-1} under these extreme conditions. The study bears upon the intrinsic interest of identifying extreme maximum temperatures and yields interesting information regarding the comfort zone of animals (including man).

1. Introduction

It is a common experience that dry sand under a full sun on a very hot summer day can be painful to the touch, and measurement would probably show that the sand surface had a temperature well in excess of 50°C (see Table 3 later regarding land surface temperatures). In contrast, maximum sea surface temperatures are observed to be in the vicinity of 306 K (33°C) only (e.g., Hastenrath and Lamb 1979; Ramanathan and Collins 1991). This leads to a number of queries regarding actual observations of extreme maximum temperatures of the land surface, what the upper limit to this temperature might be, and how well soil–atmosphere interactive models can simulate these extreme conditions. Physical considerations suggest that extreme maxima will be found at bare-soil surfaces (which implicitly have low aerodynamic roughness), where the soil is dry and has a very low albedo and low thermal conductivity. At the same time, weather conditions must be conducive to high insolation during the daytime (therefore, no clouds), low winds, and high air temperatures (e.g., in summer with warm-air advection). It is worth emphasizing our interest in the behavior of natural soils, which are assumed to be homogeneous throughout and of depth greater than a few centimeters. In contrast, car roofs, for example, made of metal with high thermal conductivity can achieve high temperatures under similar summer conditions, as specified above, mainly because they are thin (fractions of a centimeter) and overlay a medium (usually air) of much lower conductivity. In this case, the heat flux into the interior is relatively small, in contrast with a high conductivity thick soil layer where the heat flux is relatively large.

This paper reviews and describes the observational evidence under which high surface temperatures occur and utilizes realistic models of soil–atmosphere exchange so as to compute the diurnal cycle of surface temperature under extreme heating conditions. In addition, a basic theoretical approach, with some realistic assumptions, gives an indication of surface temperatures to be expected under extreme atmospheric conditions. Apart from the intrinsic interest of identifying extreme maximum temperatures, which yields interesting information regarding the comfort zone of animals (including man), the study is important in the context of assessing maximum temperatures generated in numerical models of the atmosphere.

2. Theory

We consider a bare, flat soil surface where the balance of vertical energy fluxes is represented by the surface energy balance (SEB) equation

$$H + \lambda E = R_N - G_0. \quad (1)$$

Here H is the turbulent sensible heat flux, E is the evaporation (λ is the latent heat of vaporization of water), R_N is the net radiation, and G_0 is the surface soil heat flux (all fluxes are in units of watts per square meter). A value of the surface temperature T_0 can be evaluated from Eq. (1) when each of the component fluxes is written (or parameterized) in a suitable form. The net radiation can be expressed in terms of the relevant radiative fluxes, namely,

Corresponding author address: Dr. John R. Garratt, CSIRO, Division of Atmospheric Research, Private Bag No. 1, Mordialloc, Victoria 3195, Australia.

$$R_N = (1 - \alpha)S + \epsilon R_{lw} - \epsilon\sigma T_0^4, \quad (2)$$

where α is the albedo, ϵ is the surface emissivity, and σ is the Stefan–Boltzmann constant (5.67×10^{-8} W m^{-2} K^{-4}). On the right-hand side, S is the shortwave flux (direct and diffuse components) at the surface and R_{lw} is the downward longwave flux. The turbulent fluxes are usually modeled as

$$H = \frac{\rho c_p(\theta_0 - \theta_a)}{r_{aH}} \quad (3)$$

$$E = \frac{\rho(q_0 - q_a)}{r_{aV}}, \quad (4)$$

where ρ is air density, c_p is the specific heat of air, and θ and q are potential temperature and specific humidity, respectively, with subscripts zero and a referring to surface and air (at a nominal height of a few meters). Finally, r_{aH} and r_{aV} represent aerodynamic resistances to heat and water vapor transfer, respectively. They can be written in terms of surface-layer similarity theory (see appendix A).

How can the soil heat flux G_0 be evaluated or modeled realistically? Consider for the moment the heat flux at some depth z', namely

$$G = -k_s \frac{\partial T_s}{\partial z'}, \quad (5)$$

where $T_s(z', t)$ is the soil temperature and k_s is the soil thermal conductivity (note that $k_s = \rho_s c_{ps} \kappa_s$ where ρ_s is the soil density, c_{ps} is the specific heat of soil and κ_s is the soil thermal diffusivity), which is assumed to be constant throughout the soil layer. The soil temperature is the solution of the heat diffusion equation,

$$\frac{\partial T_s}{\partial t} = \kappa_s \frac{\partial^2 T_s}{\partial z'^2}. \quad (6)$$

In numerical models, Eq. (6) can be solved numerically in finite-difference form by utilizing a number of soil levels and taking suitable initial and boundary conditions. The heat flux G_0 is then inferred from Eq. (5) with a value of $(\partial T_s/\partial z')_0$ found from the solution for $T_s(z', t)$. An alternative approach to a multilevel soil model is a force–restore method (e.g., Dickinson 1988); this utilizes a near-surface thin soil layer of temperature T_0 and a thicker reservoir layer of temperature T_B. The temperature T_0 can be described through the heat balance of the thin soil layer, namely,

$$C_g \frac{\partial T_0}{\partial t} = G_0 - \gamma(T_0 - T_B), \quad (7)$$

where C_g is the soil heat capacity per unit area (J m^{-2} K^{-1}) and the second term on the right-hand side is a parameterized form of the soil heat flux at the base of the thin surface layer. The flux G_0 is given by Eq. (1). For realistic atmospheric forcing and following the work of Bhumralkar (1975) and Blackadar (1979), C_g and γ can be represented by

$$C_g = 0.95\rho_s c_{ps}(\kappa_s/2\Omega)^{1/2} \quad (8)$$

$$\gamma = 1.18\Omega C_g, \quad (9)$$

where Ω is the angular velocity of the earth, 7.29×10^{-5} rad s^{-1}.

The above theoretical framework is the basis for the calculation of fluxes and surface temperature in numerical models of the atmosphere. It can also be used to assess the sensitivity of land surface temperatures to a range of parameters and to estimate the likely extreme maximum surface temperature occurring in nature.

It is reasonable to assume that the extreme maximum temperature will tend to occur when the incoming radiant energy is a maximum and when the absorbed shortwave and longwave fluxes are both a maximum. We set $F_0 = (1 - \alpha)S + \epsilon R_{lw}$, utilize Eq. (3), and replace potential by absolute temperatures for present purposes. Equation (1), taking account of Eq. (2), can be written

$$\left(\frac{\rho c_p}{r_{aH}}\right) T_0 + \epsilon\sigma T_0^4 = F_0 + \left(\frac{\rho c_p}{r_{aH}}\right) T_a - G_0 - \lambda E. \quad (10)$$

Note that written in this form, T_0 (the left-hand side) will tend to be large when both F_0 and T_a are large (hence, high incoming solar energy, low albedo, and high air temperature) and when G_0 and E are small (hence, low evaporation over dry soil and small soil heat fluxes). In the latter case, we can set $E = 0$ and take $G_0 = \gamma(T_0 - T_B)$ in the quasi-steady conditions prevailing near the time of maximum surface temperature [see Eq. (7)]. Note that [Eqs. (8) and (9)] γ can also be written as $0.56k_s/d$, where d is a damping depth given by $(\kappa_s/2\Omega)^{1/2}$. Equation (10) then becomes

$$\left(\frac{\rho c_p}{r_{aH}}\right) T_0 + \epsilon\sigma T_0^4 = F_0 + \left(\frac{\rho c_p}{r_{aH}}\right) T_a - \gamma(T_0 - T_B). \quad (11)$$

This shows that T_0 will tend to be maximized by reducing k_s (hence soil heat flux), that is, by considering soils of low thermal conductivity. Finally, Eq. (11) can be rearranged in the form

$$\left(\frac{\rho c_p}{r_{aH}} + \gamma\right) T_0 + \epsilon\sigma T_0^4 = F_0 + \left(\frac{\rho c_p}{r_{aH}}\right) T_a + \gamma T_B, \quad (12)$$

which is valid for dry soil. This gives guidance on the parameters and variables of significance in a numerical simulation designed to give extreme maximum surface temperatures.

3. Consideration of quantities influencing the surface temperature

In reference to Eq. (12), which is a simple version of the SEB equation in recast form, it is of interest to consider natural limits and realistic values of the various quantities affecting the surface temperature.

a. The shortwave flux

The incoming flux F_0 contains the shortwave flux S and shortwave albedo α. In nature, S is related to the solar irradiance or shortwave flux at the top of the atmosphere received on a plane normal to the direction of the radiation stream. The flux averaged over one year is called the solar constant with a value of 1367 W m^{-2}. In January, when the earth is closest to the sun, the shortwave flux at the top of the atmosphere is as high as 1410–1420 W m^{-2}. The shortwave flux received at the surface under clear skies consists of direct and diffuse contributions, but even where the sun is directly overhead, it is always less than the solar irradiance by about 10%–20% on average due to absorption and scattering of radiation by the atmosphere. In addition, the albedo of most dry soils lies in the 0.15–0.35 range; smaller values usually occur when the soil is wet (and therefore usually darker). Maximum possible values of S appear to lie close to 1100–1200 W m^{-2} (see Figs. 6.3 and 6.4 in Paltridge and Platt 1976), so that taking a minimum soil albedo of 0.15 suggests a maximum absorbed shortwave flux [$S^* = (1 - \alpha)S$] of about 1000 W m^{-2}. This value is used for guidance in the numerical simulations to be discussed later.

b. The downward longwave flux

The incoming flux also contains the downward longwave flux that, in clear skies, is determined predominantly by the humidity and temperature profile throughout the atmosphere. In numerical models of the atmosphere, the downward flux throughout the atmosphere and at the surface is computed using a detailed multi-interval band or broadband emissivity parameterization schemes (Stephens 1984). The broadband emissivity approach is used in the models discussed in section 6.

Estimates of the downward flux can be made using simple empirical formulations. These formulations generally use the screen-level air temperature, together with the associated vapor pressure in some cases, to infer the flux, and are therefore likely to be unreliable outside of the range of conditions for which they were developed. In order to estimate likely values of the flux R_{lw}, Table 1 shows estimates from three empirical relations and calculations from a numerical model with specified vertical profiles typical of atmospheric conditions at the time of high surface temperatures. Values are given for T_a in the range 298–328 K, with a screen-level humidity of 5 g kg^{-1}. It is clear that Swinbank's (1963) relation overestimates the flux, increasingly so as temperature increases. The other relations and the numerical model results give flux values in the range 320 W m^{-2} (for T_a = 298 K) to 490 W m^{-2} (for T_a = 328 K), which can be contrasted with the shortwave flux values quoted above and the outgoing blackbody longwave fluxes equal to σT_0^4.

For these extreme surface conditions, the numerical model results suggest a simple relation between flux and air temperature, suitable for use in the sensitivity analysis in the next section, with

$$R_{lw} = 5.41T_a - 1285, \qquad (13)$$

where R_{lw} is in watts per square meter and T_a is in kelvins.

TABLE 1. Values of the downward longwave flux at the surface under clear skies computed by several methods:

A: Brutsaert (1982; p. 138–139)—

$$R_{lw} = 1.24(e_a/T_a)^{1/7}\sigma T_a^4.$$

B: Linke (1970) (see Somieski et al. 1988)—

$$R_{lw} = \sigma T_a^4[0.79 - 0.174 \exp(-0.095e_a)].$$

C: Swinbank (1963)—

$$R_{lw} = 0.94 \times 10^{-5}\sigma T_a^6.$$

D: Numerical model, using a broadband emissivity method—

$$R_{lw} = \sum_{i=1}^{N} \sigma T_1^4[\epsilon_i(m + \delta m) - \epsilon_i(m)],$$

where ϵ is the emissivity, m is the optical depth for n absorbing gases, and N is the number of atmospheric layers.

In A and B, e_a is 8 hPa; in D, vertical profiles of temperature and humidity were chosen as representative of conditions conducive to high surface temperatures.

T_a (K)	A	B	C	D (model)
298	331	317	373	326
308	376	366	455	380
318	425	416	551	435
328	479	465	664	490

c. The soil heat flux

The magnitude of the soil heat flux, and hence the maximum surface temperature, is strongly dependent on the soil thermal conductivity k_s. According to the literature, minimum values of k_s for dry, natural soils tend to lie in the range of 0.1–0.2 W m^{-1} K^{-1} (Geiger 1965; Table 10).

d. Air temperatures

The maximum screen air temperatures ever recorded in the world appear to be slightly in excess of 55°C and are certainly in the range 55°–60°C (e.g., Griffiths 1972; Holford 1982).

e. Aerodynamic resistance

Values of this quantity expected in the highly unstable conditions above the heated soil surface are given in appendix A. Values are most likely in the range 100–200 s m^{-1}, as predicted by both Monin–Obukhov theory and free-convection theory, and rely on assumed values of surface heat flux of 300–500 W m^{-2} and the roughness length for temperature z_T of 0.1–1 mm (see appendix B).

4. Sensitivity of the surface temperature to soil and air properties and ambient conditions

a. Air–surface temperature difference

With the knowledge of a known observed extreme maximum air temperature at screen level (say 57°C), a suitable surface-layer formulation for the temperature profile can be used to investigate the likely maximum surface temperature. When winds are not too light (so that u_*, the friction velocity, is a physically meaningful quantity) the air–surface temperature difference ($\Delta\theta = \theta_0 - \theta_a$) can be written as (see appendix A)

$$\Delta\theta = \frac{1}{k}\left(\frac{H}{\rho c_p u_*}\right)\left[\ln\left(\frac{z}{z_T}\right) - \Psi_H\left(\frac{z}{L}\right)\right], \quad (14)$$

where definitions are given in appendix A. In light winds in the free-convective limit Eq. (14) cannot be used, and an alternative relation (see appendix A) takes the form

$$\Delta\theta = 2.15\left(\frac{H}{\rho c_p}\right)^{2/3}\left(\frac{gz_T}{\theta}\right)^{-1/3}. \quad (15)$$

The constant of proportionality is taken from Schumann (1988) and is consistent with Australian observations (e.g., Garratt 1992; ch. 3).

To compute values of $\Delta\theta$ we take $z = 2$ m (screen level), $k = 0.4$, and z_T in the range 0.1–1 mm. Maximum surface temperatures and air–surface temperature differences are likely to occur in the middle of the day when, inter alia, heat fluxes are large. However, the Ψ function increases with instability, which will tend to reduce the temperature difference. These Ψ functions are not known well at all for $z/L < -5$, but for calculation purposes, Ψ is computed for values of z/L as low as -25 (using the empirical relations described in appendix A), and a sensible heat flux of 400 W m^{-2} is used. It seems unlikely, from simple calculations and various observations, that this heat flux would be exceeded under the assumed extreme climatic conditions [Wyngaard (1991) quotes expected maximum values just less than 400 W m^{-2}]. These values of H and ζ give a friction velocity in the range 0.07–0.12 m s^{-1} (see appendix A and Table 2). Substituting into Eqs. (14) and (15) gives extreme maximum air–surface temperature differences ($\theta_0 - \theta_a \approx T_0 - T_a$) as shown in Table 2. There is a satisfactory degree of consistency between the prediction of Eq. (14) at the higher instabilities (and thus the smaller u_* values) and that of Eq. (15) for free convection. Depending upon the assumptions made (regarding the values of u_* and z_T), the extreme maximum temperature differences are likely to be in the range 32°–35°C (when $z_T = z_0 = 1$ mm) and approximately 48°–69°C (when $z_T = z_0/10 = 0.1$ mm). Smaller values of z_0 or z_T are unlikely, though a value of z_T in excess of 1 mm is possible for a roughened undulating surface. A value of several millimeters would give a temperature difference in the range of 20°–30°C.

TABLE 2. Calculated values of $\Delta\theta$, the air–surface temperature difference, under extreme instability conditions [see Eqs. (14) and (15)]. Here $z = 2$ m, $z_0 = 1$ mm, and $H = 400$ W m^{-2}.

					$\Delta\theta$	
	ζ	u_*	θ_*	ψ_H	$z_0 = z_T$	$z_0/z_T = 10$
Eq. (14)	−5	0.121	−2.9	3.2	32	48
	−10	0.097	−3.6	3.8	34	55
	−25	0.071	−4.8	4.7	35	62
Eq. (15)					32	69

In combination with a possible extreme air temperature of 57°C, the above calculations suggest an extreme maximum surface temperature in the range of approximately 90°–120°C. This prediction can be compared with calculations based on the surface energy balance approach.

b. Surface energy balance

Return to Eq. (12) and consider the sensitivity of T_0 to a number of parameters in a little more detail. By introducing Eq. (13) into Eq. (12), the SEB equation can be rewritten in the form

$$F(T_0) = \left(\frac{\rho c_p}{r_{aH}} + \gamma\right)T_0 + \sigma T_0^4 = S^* + f(T_a) + \gamma T_B, \quad (16)$$

where it is assumed that the surface behaves as a blackbody ($\epsilon = 1$), and where

$$f(T_a) = \left(\frac{\rho c_p}{r_{aH}}\right)T_a + (5.41T_a - 1285). \quad (17)$$

For specified values of γ (soil) and r_{aH} (aerodynamic) the left-hand side of Eq. (16), $F(T_0)$, can be evaluated as a function of T_0. Such curves, for T_0 in the upper range of 330–365 K, are shown in Fig. 1, where several values of r_{aH} are taken in the range 100–200 s m^{-1} (see appendix A) and $\gamma = 2.57$ W m^{-2} K^{-1} [based on a k_s value of 0.17 W m^{-1} K^{-1} and κ_s of 0.2×10^{-6} m^2 s^{-1}, and which implies a damping depth d of 0.037 m—see Eqs. (8) and (9)], the latter representing a probable minimum value for natural dry soils. These values of r_{aH} would be expected under summertime convective conditions in the middle of the day for a bare soil of aerodynamic roughness z_0 of 1 mm.

By evaluating the right-hand side of Eq. (16) for specified values of S^*, T_a, and T_B, solutions to the equation can be readily deduced and indicated on the appropriate $F(T_0)$ curve for the desired values of r_{aH}. Such solutions are shown in Fig. 1 for $S^* = 1000$ W m^{-2}, values of T_a between 298 and 328 K, and values of T_B between 290 and 310 K. The full and dashed curves sloping slightly downward from left to right join the solutions on each major curve for three values of the soil temperature. They indicate the relatively low

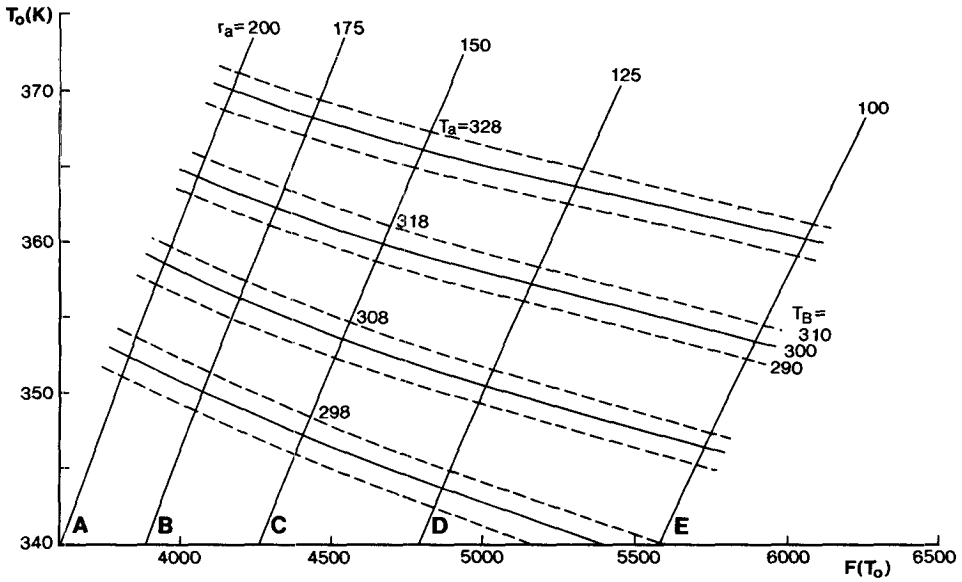

FIG. 1. Curves A–E (main curves) give the variation of $F(T_0)$, the left-hand side of Eq. (16), with surface temperature T_0, for $\gamma = 2.57$ W m^{-2} K^{-1} and five values of r_{aH} (s m^{-1}) as shown. The opposite sloping curves (secondary curves) give the solution of Eq. (16) for T_0, for $S^* = 1000$ W m^{-2}, and four values of the air temperature T_a. For each value of T_a, solutions are shown for three values of the deep-soil temperature T_B. Thus, moving along any main curve gives the sensitivity of T_0 to air temperature and deep-soil temperature; moving along the secondary curves gives the sensitivity of T_0 to the aerodynamic resistance.

sensitivity of T_0 to assumed values of r_{aH} and T_B for bare dry soil. Note that T_0 is expected to be in the 340–370-K range for air temperatures in the 298–328-K range and a shortwave flux of about 1000 W m^{-2}. At the same time, air–surface temperature differences are about 30°–40°C.

The right-hand side of Eq. (16) has been calculated for a range of S^* (700–1100 W m^{-2}) and T_a (298–328 K) for assumed values of γ (2.57 W m^{-2} K^{-1}), r_{aH} (100 s m^{-1} and 200 s m^{-1}), and T_B (300 K). These values are chosen as being conducive to high surface temperatures. Each calculated value [of the right-hand side of Eq. (16)] has an associated value of T_0 given by the solution of Eq. (16) (the solution actually lies on either of curves A or E in Fig. 1). The solutions are shown in Fig. 2 as isopleths of T_0 at 5-K intervals for the above ranges in T_a and S^*. Thus, the diagram gives a quantitative indication of how T_0 is likely to vary: (i) for S^* varying at a given air temperature and (ii) for T_a varying at a given shortwave flux. For $S^* = 1000$ W m^{-2}, values of T_0 in the vicinity of 365 K (92°C) are indicated for an air temperature of 330 K (57°C).

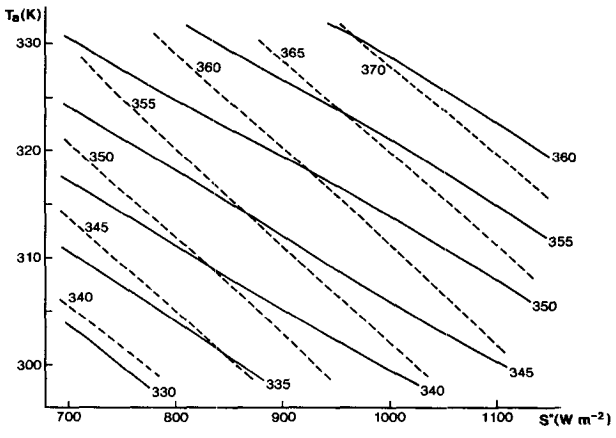

FIG. 2. Solutions of Eq. (16), in terms of isopleths of T_0, for variations in air temperature and absorbed shortwave flux; values of $\gamma = 2.57$ W m^{-2} K^{-1}, $r_{aH} = 100$ s m^{-1} (continuous curves) and 200 s m^{-1} (pecked curves), and $T_b = 300$ K have been assumed.

Now the observational evidence for extreme maximum land surface temperatures will be reviewed, and then the results of numerical simulations will be described.

5. Observations of extreme maximum land surface temperatures

Observations of extreme maximum land surface temperatures are not commonly reported in the literature. Table 3 summarizes some relevant reports, with air temperatures given where possible. The indirect values of T_0 are those where the author has surmised that such a value was probably measured; otherwise, values reflect direct observations—in the early days, usually using dry-bulb thermometry, and most recently, using infrared radiometers. There are several values in the vicinity of, or in excess of, 70°C; two quoted values were made at small depths in the soil, and later numerical results (section 6b) were used to

TABLE 3. Observations of extreme maximum surface temperatures (in degrees Celsius) taken from the literature. Also shown are air temperatures near the time of the observed surface temperature. Both direct and indirect surface observations are shown (for an explanation see the text). Johnson and Davies (1927) is denoted JD1927 and Cloudsley-Thompson and Chadwick (1964) is CC1964. Garratt's observations were made at Aspendale during February 1991 using an infrared radiometer. Names in parentheses are the quoted source of the relevant observations. Note that Sutton (1953, p. 194) refers to Sinclair's (1922) observations, Oke (1987, p. 82) refers to Peel's (1974) observations, and Deacon (1969, p. 50) refers to West's (1952) observations.

Reference	Surface	T_0 direct	T_a	T_0 Indirect	T_a
CC1964 (p. 20, 21)	desert	≈80	≈40		
Peel (1974)	desert	79.3	40–47		
Sinclair (1922)	desert	71.5*	≈43		
JD1927					
(Field)	soil	69	43		
Geiger (1965)					
(Neubauer)	desert	60.2**			
Garratt					
(unpublished)	sandy loam	56–61	36–39		
Rose (1968, Fig. 9)	mixed soil	≈55	≈30		
Chang (1958)					
(Yakuwa)	sand	54			
West (1952)	sandy loam	≈53			
Geiger (1965)	soil			50–65	
(Huber)	?			70	
(Vaartaja)	?			63	
JD1927	sand			55	

* Refers to a depth of 4 mm – the estimated T_0 (see text) is 74°C.
** Depth of 15 mm – estimated T_0 is 70°C.

correct these to the surface. Interestingly, Johnson and Davies (1927) suggested a possible upper limit of about 93°C occurring with extreme air temperatures (the most extreme ever observed) of 57°C. There is no direct evidence of any natural surface with temperatures as high as this, though model simulations do get close (see next section), as do the calculations made in the previous section.

Observations described above are local and do not include remote measurements made from aircraft or satellite. The author has access to measurements made from an aircraft over the desert in central Australia (A. J. Prata, private communication), showing extreme maxima of about 62°C. Satellite observations made over large areas [e.g., the Advanced Very High-Resolution Radiometer (AVHRR) on the National Oceanic and Atmospheric Administration (NOAA) satellites] are readily available but do not register temperatures above about 54° to 58°C due to saturation of the radiometer channels (because of atmospheric effects and surface emissivities of less than one, these upper values should be increased by several degrees).

6. Numerical model calculations

a. Surface temperature and fluxes

Two models have been used. The first is a one-dimensional (1D) stand-alone boundary-layer–soil model (model I) utilizing a force–restore scheme for evaluating surface temperature (and soil moisture), and the second is a 1D version of a mesoscale dynamical model linked with a multilevel soil model (model II)—in all, 25 soil levels were used, with 1-mm resolution near the surface. Numerical solution of the full soil moisture and heat diffusion equations is carried out in the latter case. In both models, the longwave radiative fluxes are calculated using a broadband emissivity scheme typical of many mesoscale models of the atmosphere (e.g., see Somieski et al. 1988). The surface flux of heat and the friction velocity are calculated using a surface-layer scheme based on Monin–Obukhov theory.

Each model was integrated typically for a period of 2 days, and initialized with climatological atmospheric profiles of temperature and humidity. For clear skies, solar forcing was chosen to give the maximum incoming shortwave fluxes in excess of 1100 W m^{-2}, and adjustment of the surface albedo allowed the value of the absorbed shortwave flux to be varied from one run to the next. The surface roughness length was set at 1 mm, the surface emissivity at unity [natural soils appear to have emissivities in the range 0.9–0.99 (e.g., Sutherland 1986), which, if included in the present calculations, raise maximum temperatures by several degrees], and the geostrophic wind was held constant at 5 m s^{-1}. The minimum atmospheric level in each model was 10 m. Numerous simulations were performed with values of z_0, k_s, κ_s (hence, γ in the force–restore model), maximum shortwave flux, and initial air temperature varied so as to assess those combinations that lead to near extreme maximum surface temperatures.

Table 4 summarizes the results of four runs using model II where the thermal conductivity is varied over

TABLE 4. Variation in the calculated maximum surface temperature using model II with the assumed soil thermal conductivity. Some flux values at the time of maximum temperature are also shown. The k_s value of 0.17 W m^{-1} K^{-1} is taken as a most probable minimum value for natural soils.

k_s (W m^{-1} K^{-1})	γ (W m^{-2} K^{-1})	T_0 (K)	R_N	H (W m^{-2})	G_0
0.17	2.57	345.4	623	471	149
0.083	1.28	347.5	604	495	105
0.041	0.64	349.2	610	516	92
0.021	0.32	350.5	598	530	65

(almost) an order of magnitude—the value of the maximum T_0 is not too sensitive to the choice of k_s. The literature suggests minimum values in the range 0.1–0.2 W m^{-1} K^{-1} for dry, natural soils, and a value of 0.17 W m^{-1} K^{-1} has been taken for all remaining simulations. An interest is taken in evaluating the extreme surface temperature occurring for a realistic combination of extreme values of the primary (S^*, T_a) and secondary (r_{aH}, k_s, deep-soil temperature) forcing variables—that is, values consistent with known physical properties of air and soil and with observations. To this end, the minimum value of soil thermal conductivity was taken as 0.17 W m^{-1} K^{-1} and the maximum absorbed shortwave flux as 1000 W m^{-2}. In order to generate a maximum air temperature in the observed range of 55°–60°C, the initial air temperatures were simply increased by 25°C above the climatological profile values. With this combination, the simulation using the multilevel soil scheme (model II) gave a maximum air temperature of about 57°C, with a maximum surface temperature of 93°C occurring 1–2 h earlier. With the force–restore model (model I), the maximum air and surface temperatures were 56° and 88°C, respectively, and the bulk soil temperature was in the range 304–308 K over the 2-day simulation period. In addition, the maximum net radiation was close to 500 W m^{-2}, with about 350 W m^{-2} taken up as sensible heat flux into the atmosphere and the remainder (150 W m^{-2}) going into the soil. Figure 3 shows the results of this simulation for both models. Under these imposed extreme conditions (with zero evaporation), small flux differences produce only minor differences in air temperature and a difference in maximum surface temperature of 5°C.

These model results suggest that under extreme, but realistic, conditions, surface temperatures of 90°C or slightly more are feasible, though observations revealing such high values are unknown to the author.

b. Subsurface temperature profiles

References have been made in the literature to soil temperature measurements made at small depths of several millimeters only (see Table 3). At the time of maximum surface temperature, these subsurface values are likely to be several degrees lower than the surface value. Two such observations were tentatively corrected in the table based on numerical simulations. Soil temperature profiles can be calculated in the high-resolution model (model II). The soil profile corresponding to the simulation shown in Fig. 3 is given in Fig. 4 [curve (a)], together with two profiles calculated earlier [curve (b)] and later [curve (c)] in the day. These results reveal large temperature gradients near the surface, close to 0.6°C mm^{-1} near the time of maximum surface temperature. Thus, the observation of 71.5°C at 4-mm depth measured by Sinclair probably implies a $T_0 \approx 74$°C; the observation of 60.2°C at 15-mm depth quoted by Geiger implies a $T_0 \approx 70$°C (see Table 3).

7. Discussion

Simplification of the SEB equation allows the sensitivity of the land surface temperature to a range of

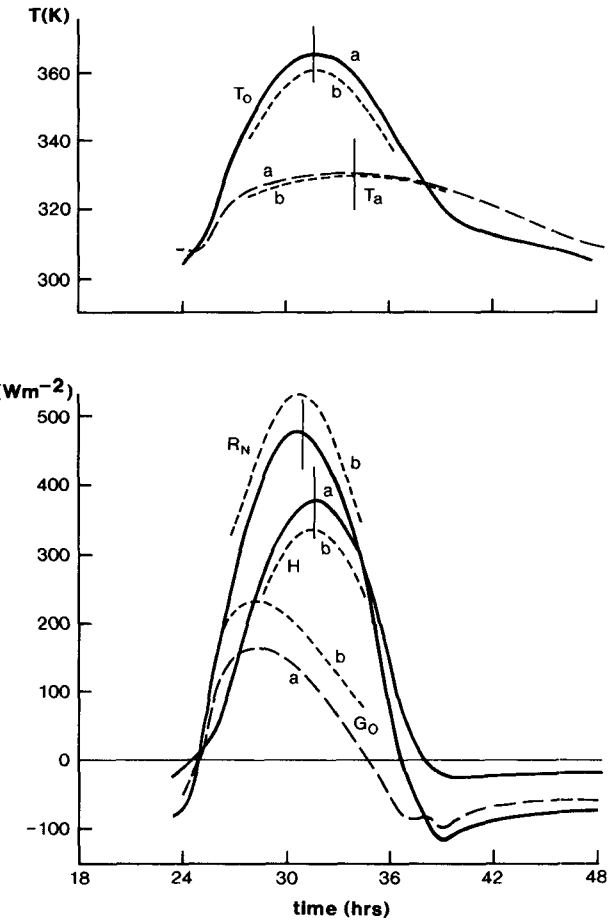

FIG. 3. Diurnal variations of temperatures and fluxes for initial and boundary conditions giving an extreme maximum surface temperature of 366 K (93°C)—simulations using model II with high-resolution soil scheme [full and long-pecked curves (a)] and model I with force–restore scheme [short-pecked curves (b), shown only in part]. Faint vertical bars indicate the position of the relevant maximum. Time axis is in hours from the commencement of the simulation.

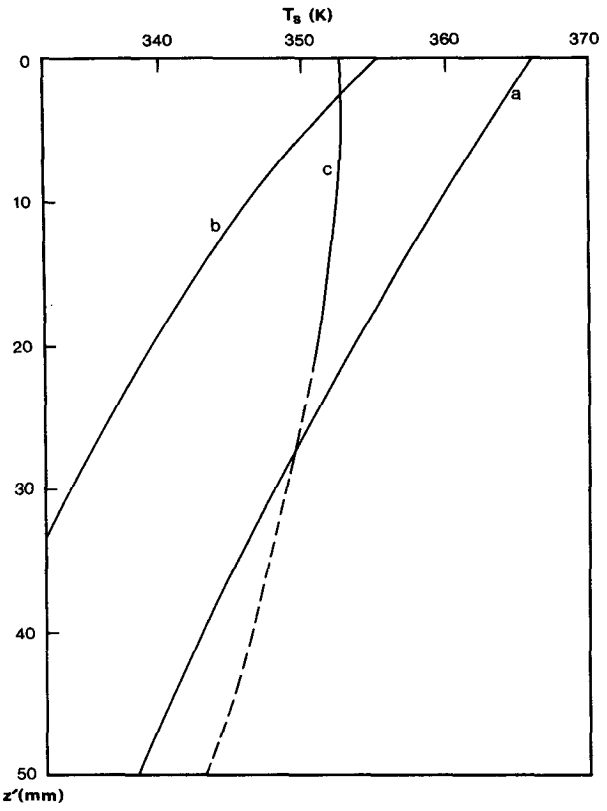

FIG. 4. Vertical profiles of temperature in the first 50 mm of soil calculated using model II, for the same simulation conditions as those appropriate to Fig. 3; curve (a) is at the time of maximum surface temperature. Curves (b) and (c) are for 3 h earlier and later, respectively.

soil and atmospheric variables to be assessed and quantified. These variables include the primary forcing variables S^* (the absorbed shortwave flux) and T_a (the screen air temperature) and the secondary forcing variables r_{aH} (the aerodynamic resistance), T_B (the deep soil temperature), and k_s (the soil thermal conductivity). Consideration of the soil–atmosphere system, together with the observations, allows realistic maximum values of S^* and T_a and a minimum value of k_s to be set. These, together with expected values of r_{aH} and T_B, suggest that land surface temperatures in the vicinity of 90°C could occur. Numerical simulations using interactive atmosphere–soil models, with both two-layer and multilayer soil schemes, confirm this prediction. With a maximum daytime absorbed shortwave flux of about 1000 W m^{-2} and air temperature of about 57°C, and with an aerodynamic roughness length of 1 mm and a soil thermal conductivity of 0.17 W m^{-1} K^{-1}, a maximum surface temperature of 93°C was achieved.

There is probably no observation in existence that has been taken under such extreme conditions. Certainly, a survey of the literature reveals numerous observations of extreme maximum land surface temperatures in the range of 50°–70°C, with some evidence of values around 80°C. Interestingly, Johnson and Davies (1927) commented that even where the air temperature approached the highest ever observed (57.2°C at that time), "it is unlikely that the surface temperature of the soil will ever exceed [93.3°C]."

The above numerical atmosphere–soil schemes are common to many mesoscale and general circulation models of the atmosphere. Thus, the results are highly relevant to short-term regional simulations and longer-term regional and global simulations of weather and climate. Together with the observational evidence, they serve to set a probable upper limit to the maximum land surface temperature in the range 80°–93°C. Under less extreme climatic conditions, dry soil of low thermal conductivity will experience significantly smaller surface temperatures and, when wet or covered in transpiring vegetation, maximum temperatures will rarely exceed 40°C or so.

Acknowledgments. Thanks to Mrs. Eva Kowalczyk and Mr. Paul Krummel for performing the various model simulations used in this paper.

APPENDIX A

Calculation of Friction Velocity and Aerodynamic Resistances

The surface fluxes are related to the turbulent scaling parameters u_*, θ_*, and q_* through

$$\tau = \rho u_*^2, \tag{A1}$$

$$H = -\rho c_p u_* \theta_*, \tag{A2}$$

$$E = -\rho u_* q_*. \tag{A3}$$

Here τ is the surface stress (momentum flux), H is the sensible heat flux (positive during daytime convective conditions), and E is positive for evaporation. The turbulent scaling parameters are an integral part of the Monin–Obukhov theory of the surface layer (e.g., Garratt 1992; chapter 3) and are related to mean field variables through the following,

$$u_* = \frac{k u_a}{\ln(z/z_0) - \Psi_M(z/L)} \tag{A4}$$

$$\theta_* = \frac{k\mathrm{Pr}^{-1}(\theta_a - \theta_0)}{\ln(z/z_T) - \Psi_H(z/L)}. \tag{A5}$$

A similar relation to Eq. (A5) for q_* can be written with $\theta_a - \theta_0$ replaced by $q_a - q_0$. In the above, k is von Kármán's constant, Pr is a neutral turbulent Prandtl number, z is height, z_0 and z_T are aerodynamic roughness and temperature surface scaling lengths, respectively, and L is the Monin–Obukhov stability length defined in terms of u_* and θ_* $\{L = -u_*^3[k(g/\theta)(H/\rho c_p)]^{-1}\}$. Note that θ_0 and θ_a are the values of potential temperature at the height z_T (not z_0) and a level usually several meters above the ground within the atmospheric surface layer, respectively.

The surface heat flux can be written in the form

$$H = \rho c_p C_H u_a(\theta_0 - \theta_a) \quad \text{(A6)}$$

or

$$H = \frac{\rho c_p(\theta_0 - \theta_a)}{r_{aH}}, \quad \text{(A7)}$$

where C_H is a bulk heat transfer coefficient and $r_{aH} = (C_H u_a)^{-1}$ is an aerodynamic resistance to heat transfer. Note that reference to Eqs. (A1)–(A5) shows that

$$r_{aH}^{-1} = k^2 u_a\{[\ln(z/z_0) - \Psi_M(z/L)] \times [\ln(z/z_T) - \Psi_H(z/L)]\}^{-1}. \quad \text{(A8)}$$

It is usual to assume that the resistance to water vapor transfer $r_{aV} = r_{aH}$.

The Ψ functions in Eqs. (A4) and (A5) can be readily written in terms of the gradient functions Φ defined as

$$\Phi_M = \left(\frac{kz}{u_*}\right)\frac{\partial u}{\partial z}, \quad \Phi_H = \left(\frac{kz}{\theta_*}\right)\frac{\partial \theta}{\partial z}.$$

The Ψ and Φ functions are related by

$$\Psi = \int [1 - \Phi(\zeta)]d(\ln\zeta), \quad \text{(A9)}$$

where $\zeta = z/L$. The Φ functions broadly take the form, for $\zeta \leq 0$,

$$\Phi_M = (1 - \gamma_1\zeta)^{-1/4} \quad \text{(A10)}$$

$$\Phi_H = \Pr(1 - \gamma_2\zeta)^{-1/2}. \quad \text{(A11)}$$

It is acceptable to take $k = 0.4$, $\Pr = 1$, $\gamma_1 = \gamma_2 = 16$ (e.g., Garratt and Pielke 1989). Substitution of Eqs. (A10) and (A11) into Eq. (A9) yields, for unstable conditions,

$$\Psi_M(\zeta) = 2\ln\left[\frac{(1+x)}{2}\right] + \ln\left[\frac{(1+x^2)}{2}\right] - 2\tan^{-1}x + \frac{\pi}{2}, \quad \text{(A12)}$$

where $x = \Phi_M^{-1}$ and

$$\Psi_H(\zeta) = 2\ln\left[\frac{(1+y)}{2}\right], \quad \text{(A13)}$$

where $y = \Phi_H^{-1}$. For small z_0 (e.g., bare soil), the lower limit of integration on the right-hand side of Eq. (A9) can be set to zero rather than z_0/L.

The above formulations serve as a basis for the calculation of friction velocity and surface heat flux in numerical models of the atmosphere, including those used in the discussion in section 6.

For $\zeta < -5$, Φ functions are not well known, so in the numerical model, the degree of instability is limited to this value (this assumption does not have a significant impact upon the calculations). Actually, this limitation also serves a very useful practical purpose. Reference to the denominator in Eq. (A4) shows that for large z_0, the magnitude of the denominator will approach zero if ψ, and hence $-\zeta$, is too large. The value of $\zeta = -5$ (where $\psi_M = 2.07$, $\Psi_H = 3.22$) is a safe minimum value to use in the model.

For the purposes of evaluating the resistance r_{aH} in the convective conditions likely to occur with extreme maximum surface temperatures, ζ is taken as low as -25. At these instabilities, values of H probably lie in the range 300–500 W m^{-2}. Noting from Eq. (A8) that r_{aH} can also be written

$$r_{aH} = (ku_*)^{-1}[\ln(z/z_T) - \Psi_H(\zeta)], \quad \text{(A14)}$$

then r_{aH} has values indicated in Table A1. The values of u_* follow immediately from the assumed values of H and ζ, and two values of z_T, 0.1, and 1 mm are taken to encompass the range suggested in appendix B.

In light winds, in the limit of free convection, the Monin–Obukhov theory is invalid and Eq. (A14) cannot be used. Typical values of r_{aH} in the free convective limit can be readily evaluated by appeal to Eq. (A7) and a relation for the heat flux [an alternative form to Eq. (A6)] based on earlier work by Prandtl and Priestley and discussed recently in Schumann (1988). That is,

$$\frac{H}{\rho c_p} = 0.32\left(\frac{gz_T}{\theta}\right)^{1/2}\Delta\theta^{3/2}, \quad \text{(A15)}$$

so that computed values of H from specified values of $\Delta\theta$ imply a value of r_{aH}, as shown in Table A1.

Reference to Table A1 shows good consistency in the r_{aH} values, with the range 100–200 s m^{-1} likely at the time of maximum surface temperature for the assumed values of z_T.

TABLE A1. Values of r_{aH} to be expected under convective conditions over bare dry soil near the time of maximum surface temperature are shown. The u_* values are based on values of $\rho = 1.15$ kg m^{-3}, $\theta = 303$ K, $g = 9.81$ m s^{-2}, and $c_p = 1006$ J kg^{-1} K^{-1}.

			r_{aH} (s m^{-1})	
	H (W m^{-2})	u_* (m s^{-1})	$z_0/z_T = 1$ $z_T = 1$ mm	$z_0/z_T = 10$ $z_T = 0.1$ mm
$\zeta = -5$	300	0.110	100	152
	400	0.121	91	139
	500	0.130	85	129
$\zeta = -10$	300	0.088	108	173
	400	0.097	98	157
	500	0.104	91	147
$\zeta = -25$	300	0.065	112	200
	400	0.071	102	183
	500	0.076	95	171
Free convection	300		108	232
	400		93	200
	500		90	195

APPENDIX B

Values of z_0 and z_T for Bare Soils

In aerodynamically rough flow, where the roughness Reynolds number ($Re_* = u_* z_0/\nu$, ν being the kinematic viscosity of air) is >1, most z_0 values found in the literature for bare soils are about 1 mm. Larger values are likely for a roughened undulating surface, but for the idealized flat surfaces conducive to high surface temperatures in convective conditions, the z_0 value is likely to be within a factor of 2–3 of 1 mm. Many text books give tables of typical z_0 values for a range of surface types and often reproduce (without due reference) earlier published values. For example, Oke (1987; Table 2.2) gives a value of 0.3 mm for "sand, desert" probably related to the value found by Calder over a flat desert region near Karachi and discussed by Deacon (1953; appendix 1). Oke also quotes values of 1–10 mm for "soils" in general. In the Wangara report (Clarke et al. 1971) a value of z_0 equal to 1.2 mm was evaluated from wind profiles for station 5, located in a flat, bare-soil semiarid region of southeast Australia with little or no vegetation.

In highly convective conditions, when winds are light with u_* in the range 0.07–0.13 m s^{-1} (see appendix A), the maximum Re_* is likely to be about 10. Available information (Garratt and Hicks 1973; Brutsaert 1982, ch. 4; Garratt 1992, ch. 4) shows that the ratio z_0/z_T is a function of Re_* and lies in the range of approximately 1–7.4. This range is suggested for both bare and vegetated surfaces from light winds to moderate to strong winds. At values of Re_* in the range 1–10 the ratio probably lies in the lower part of the range.

Values of z_0, and hence z_T, are likely to be much smaller in aerodynamically smooth flow. Under these conditions the main roughness elements are buried within a viscous sublayer of depth $\delta \approx 5\nu/u_*$ (Schlichting 1979; ch. 20). Taking u_* in the range 0.05–0.15 m s^{-1} gives $\delta \approx 0.1$–0.3 mm, suggesting that smooth flow is unlikely in light-wind convective conditions (we assume that the dominant soil particles will have dimensions up to several millimeters at least, consistent with z_0 = 1 mm in rough flow).

REFERENCES

Bhumralkar, C. M., 1975: Numerical experiments on the computation of ground surface temperature in atmospheric general circulation models. *J. Appl. Meteor.*, **14,** 1246–1258.

Blackadar, A. K., 1979: High-resolution models of the planetary boundary layer. *Advances in Environmental Science and Engineering,* Vol. 1, J. R. Pfafflin and E. N. Zeigler, Eds., Gordon and Breach, 50–85.

Brutsaert, W., 1982: *Evaporation into the Atmosphere.* Reidel, 299 pp.

Chang, J.-H., 1958: *Ground Temperature,* Vol. 1. Harvard University Press, 300 pp.

Clarke, R. H., A. J. Dyer, R. R. Brook, D. G. Reid, and A. J. Troup, 1971: The Wangara experiment: Boundary layer data. CSIRO Division of Meteorological Physics Tech. Paper No. 19, 21 pp (+ tables).

Cloudsley-Thompson, J. L., and M. J. Chadwick, 1964: *Life in Deserts.* Foulis & Co., 218 pp.

Deacon, E. L., 1953: Vertical profiles of mean wind in the surface layers of the atmosphere. Geophys. Memoirs No. 91, Meteorological Office, H. M. Stationery Office, 68 pp.

——, 1969: Physical processes near the surface of the earth. *World Survey of Climatology,* Vol. 2. Elsevier 39–104.

Dickinson, R. E., 1988: The force–restore model for surface temperatures and their generalizations. *J. Climate,* **1,** 1086–1097.

Garratt, J. R., 1992: *The Atmospheric Boundary Layer.* Cambridge University Press, 315 pp.

Garratt, J. R., and B. B. Hicks, 1973: Momentum, heat and water vapour transfer to and from natural and artificial surfaces. *Quart. J. Roy. Meteor. Soc.,* **53,** 45–57.

——, and R. A. Pielke, 1989: On the sensitivity of mesoscale models to surface-layer parameterization constants. *Bound.-Layer Meteor.,* **48,** 377–387.

Geiger, R., 1965: *The Climate Near the Ground.* Harvard University Press, 611 pp.

Griffiths, J. F., (Ed.), 1972: *Climates of Africa. World Survey of Climatology.* Vol. 10. Elsevier, 604 pp.

Hastenrath, S., and P. J. Lamb, 1979: *Climatic Atlas of the Indian Ocean. Part I: Surface Climate and Atmospheric Circulation.* University of Wisconsin Press, 97 Charts.

Holford, I., 1982: *The Guinness Book of Weather Facts and Feats.* 2d ed. Guinness Superlatives, Ltd., 253 pp.

Johnson, N. K., and E. L. Davies, 1927: Some measurements of temperatures near the surface in various kinds of soils. *Quart. J. Roy. Meteor. Soc.,* **53,** 45–57.

Linke, F., 1970: Meteorologisches Taschenbuch. II: Band, Neue Ausgabe, Akademische Verlagesellschaff, Leipzig.

Oke, T. R., 1987: *Boundary Layer Climates.* 2d ed., Methuen, 435 pp.

Paltridge, G. W., and C. M. R. Platt, 1976: *Radiative Processes in Meteorology and Climatology.* Elsevier, 318 pp.

Peel, R. F., 1974: Insolation weathering: Some measurements of diurnal temperature changes in exposed rocks in the Tibesti region, central Sahara. *Z. Geomorph. N. F.,* Suppl. Bd. **21,** 19–28.

Ramanathan, V., and W. Collins, 1991: Thermodynamic regulation of ocean warming by cirrus clouds deduced from observations of the 1987 El Niño. *Nature,* **351,** 27–32.

Rose, C. W., 1968: Water Transport in soil with a daily temperature wave I: Theory and experiment. *Aust. J. Soil Res.,* **6,** 31–44.

Schlichting, H., 1979: *Boundary-Layer Theory.* 7th ed. McGraw-Hill, 817 pp.

Schumann, U., 1988: Minimum friction velocity and heat transfer in the rough surface layer of a convective boundary layer. *Bound.-Layer Meteor.,* **44,** 311–326.

Sinclair, J. G., 1922: Temperatures of the soil and air in a desert. *Mon. Wea. Rev.,* **50,** 142–144.

Somieski, F., P. Koepke, K. T. Kriebel, and R. Meerkotter, 1988: Improvements of simple radiation schemes for mesoscale models: A case study. *Beit. Phys. Atmos.,* **61,** 204–218.

Stephens, G. L., 1984: The parameterization of radiation for numerical weather prediction and climate models. *Mon. Wea. Rev.,* **112,** 826–867.

Sutherland, R. A., 1986: Broadband and spectral emissivities (2–18 μm) of some natural soils and vegetation. *J. Atmos. Oceanic Technol.,* **3,** 199–202.

Sutton, O., 1953: *Micrometeorology.* McGraw-Hill, 333 pp.

Swinbank, W. C., 1963: Long-wave radiation from clear skies. *Quart. J. Roy. Meteor. Soc.,* **89,** 339–348.

West, E. S., 1952: A study of the annual soil temperature wave. *Aust. J. Sci. Res.,* Ser. A, **5,** 303–314.

Wyngaard, J. C., 1991: On the maintenance and measurement of scalar fluxes. *Land Surface Evaporation (Measurement and Parameterization),* Springer-Verlag, 199–229.